

Technical Note

Numerical Investigation on the Residual Ultimate Strength of Central-Cracked Stiffened Plates under Tensile and Bending Loads Using XFEM

Guangzhong Liu ^{1,*}, Zhenting Chen ¹ and Jiahao Zhou ²

¹ School of Ocean Science and Engineering, Shanghai Maritime University, Shanghai 200135, China

² PetroChina SIPG Energy Co., Ltd., Shanghai 201306, China

* Correspondence: gzliu@shmtu.edu.cn

Abstract: The present paper aims to study the crack propagating behavior of a stiffened plate under tensile and bending displacement load loads. The extended finite element method (XFEM) is used to analyze the residual ultimate strength of stiffened plates with a central crack. The quasi-static crack growth process is simulated by software ABAQUS. The validity of the grid is validated by the plate with a central crack. The numerical method is validated by comparing the fatigue crack growth rate of the round compact tension specimen (RCT) results of the extended finite element with experiment values. Influential parameters, including the size of the stiffened plates, heights of the stiffeners is varied, and uniaxial tensile and four-point bending models are analyzed. The results show that ultimate strength is reduced by the action of tensile and bending loads. The bottom plate and stiffener are destroyed with crack propagation, successively. With the increase in stiffener height, the crack resistance will also increase, thus restraining the central crack growth of stiffened plates.

Keywords: extended finite element method; stiffened plate; cracking process; the ultimate strength



Citation: Liu, G.; Chen, Z.; Zhou, J. Numerical Investigation on the Residual Ultimate Strength of Central-Cracked Stiffened Plates under Tensile and Bending Loads Using XFEM. *J. Mar. Sci. Eng.* **2023**, *11*, 302. <https://doi.org/10.3390/jmse11020302>

Academic Editor: Joško Parunov

Received: 19 December 2022

Revised: 5 January 2023

Accepted: 5 January 2023

Published: 1 February 2023



Copyright: © 2023 by the authors. Licensee MDPI, Basel, Switzerland. This article is an open access article distributed under the terms and conditions of the Creative Commons Attribution (CC BY) license (<https://creativecommons.org/licenses/by/4.0/>).

1. Introduction

Ships work constantly under complex sea conditions, suffering from the combined action of wind, waves and current. In order to cope with the complex working conditions of the ocean, many structures with increased ultimate strength have been proposed, such as stiffened X-joints [1,2] and the stiffener [3]. Stiffened plates are the basic components of ship hull, and the existence of cracks will reduce the ultimate strength of structural components and eventually endanger the entire hull security. Thus, crack propagation in steel structures cannot be prevented. Predicting the residual ultimate strength of cracked structures is of crucial importance for ships' health monitoring and repair policy [4,5]. Residual ultimate strength analysis of stiffened plates with crack was the subject of many studies in the past years. Therefore, conducting research on the residual ultimate strength of cracked stiffened plates is essential for the reliability of ship structures during service.

Over years, researchers have devoted time to the development of efficient numerical methods for crack growth modeling, such as the boundary element method [6,7], mesh free method [8,9], finite element method (FEM) [10,11] and extended finite element method (XFEM) [12–14]. Among these methods, XFEM has gradually become the most popular method to study crack growth problems. In XFEM, as a crack grows, there is no need for re-meshing and refinement work. Fries [15] modified the standard XFEM approximation with a ramp function to overcome the inherit problem lying in blending elements, so optimal convergence rate and high accuracy can be achieved, the method is frequently referred to as corrected XFEM. Till now, the XFEM has been applied in various fracture problems including the cohesive crack propagation [16,17], crack growth with frictional contact [18,19], elastodynamic crack propagation [20], branched and intersecting crack growth [21], and three dimension crack propagation [22], even heat transfer problem [23].

In the past, some studies on residual ultimate strength of stiffened plates with cracks under different stress conditions have been carried out. Shi et al. [24] determined the residual ultimate strength of cracked steel stiffened plates subjected to axial compression through numerical calculation. Poknam et al. [25] studied the influence of cracks on the residual ultimate strength of cracked continuous stiffened plates under combined lateral pressure and compression in the plate. Zhenfei et al. [26] used tension experiments and electrical measurements for measuring the ultimate strength, failure mode, and strain-evolution process of stiffened plates. Kang et al. [27] analyzed the influence of the residual ultimate strength of cracked stiffened plates under cyclic load on the bearing capacity of stiffened plates. Huwei et al. [28] analyzed the ultimate strength and fracture failure of hull stiffened plates based on plastic accumulation have been studied under cyclic compression and compression–tension load.

From the research work carried out so far on the residual ultimate strength of stiffened plates with cracks, it is observed that the problems with crack resistance in the presence of different working conditions (uniaxial tensile and four-point bending conditions) have not been given much attention. Studying the crack resistance of stiffened plates in different working conditions are inevitable. The relationship between the reaction force and deformation is output, which can be used to characterize the crack resistance of stiffened plates. In addition, XFEM has been used to deal with such problems. The numerical method using ABAQUS 2020 [29] will be validated by the RCT specimen. In the present work, two numerical models are presented to show the residual ultimate strength of a stiffened plate with a central crack.

This paper is organized as follows: Description of XFEM formulation in software ABAQUS for crack problem in Section 2. Followed by a detailed information of two validate case which validate the correctness of the mesh and method in Section 3. In Section 4, numerical results of tensile and four-point bending model are presented, the effect of variations in the stiffener size is investigated. Finally, main conclusions are summarized as Section 5.

2. Numerical Formulation

2.1. Model Problem Definition

Consider a body in the state of equilibrium with the boundary conditions in the form of traction and displacement conditions, as depicted in Figure 1.

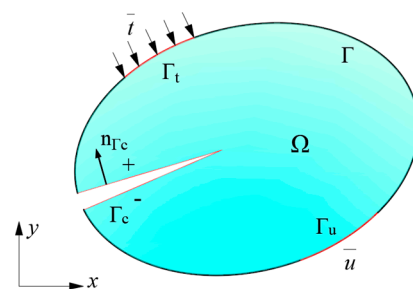


Figure 1. A body in a state of elastostatic equilibrium.

The strong form of the equilibrium equation can be written as:

$$\nabla \cdot \sigma + b = 0 \text{ in } \Omega \tag{1}$$

where ∇ is the gradient operator, σ is the Cauchy stress, and b is the body force. The behavior of the bulk material is assumed to be linear elastic, the constitutive relation is defined as $\sigma = D \cdot \varepsilon$.

With the following boundary conditions:

$$\begin{aligned} u &= \bar{u} & \text{on } \Gamma_u \\ \sigma \cdot n_\Gamma &= \bar{t} & \text{on } \Gamma_t \end{aligned} \tag{2}$$

where, n_Γ is the outward unit normal vector to the external boundary Γ , and \bar{t} is the prescribed load vector on the boundary Γ_t , \bar{u} is the prescribed displacement on the boundary Γ_u .

The variational formulation of the boundary value problem can be defined as:

$$W^{int} = W^{ext} \tag{3}$$

Or

$$\int_{\Omega} \sigma \cdot \delta \varepsilon \, d\Omega = \int_{\Omega} f^{cb} \cdot \delta u \, d\Omega + \int_{\Gamma_t} f^t \cdot \delta u \, d\Gamma \tag{4}$$

2.2. XFEM Discretization

XFEM is based on the partition of unity method, and uses rich functions to enrich the local elements, so as to approximate the displacement of the standard finite element to simulate the discontinuity between cracks and the singularity of the crack tip. ABAQUS2020 only introduces the Heaviside enhancement function, not the crack tip branch functions. Thus, as for 2D-corrected XFEM, displacement approximation in ABAQUS takes the form:

$$u^h(x) = \sum_{j \in N} N_j(x) u_j + \sum_{k \in M} N_k(x) H(x) a_k \tag{5}$$

As shown in Figure 2, N is the nodes set in the mesh; M is the node set belonging to the split element intersected with the crack. In Equation (5), u_j is the classical finite element displacement; $N_j(x)$ and $N_k(x)$ are standard FE shape functions; a_k is the nodal unknowns added to the M set of nodes. $H(x)$ is the Heaviside function used to model the discontinuity in displacement, which takes +1 on one side of the crack surface and -1 on the other side.

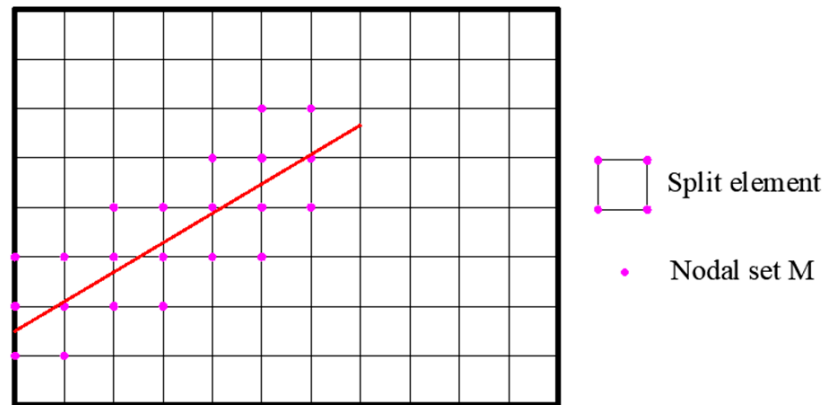


Figure 2. Nodal subsets and element types.

Discretization of Equation (4) using the XFEM procedure Equation (5) results in a discrete system of linear equilibrium equations:

$$Ku^h = f \tag{6}$$

where K is the stiffness matrix, u^h is the vector of degrees of nodal freedom (for both classical and enriched ones) and f is the vector of external force. The global matrix and

vectors are calculated by assembling the matrix and vectors of each element. K and f for each element e are defined as

$$K_{ij}^e = \begin{bmatrix} K_{ij}^{uu} & K_{ij}^{ua} \\ K_{ij}^{au} & K_{ij}^{aa} \end{bmatrix} \tag{7}$$

$$f_i^e = \{f_i^u \quad f_i^a\}^T \tag{8}$$

And u^h is the vector of nodal parameters:

$$u^h = \{u \quad a\}^T \tag{9}$$

with

$$K_{ij}^{rs} = \int_{\Omega_e} (B_i^r)^T D B_s^j d\Omega \quad (r, s = u, a) \tag{10}$$

$$f_i^u = \int_{\Gamma_t} N_i f^t d\Gamma \tag{11}$$

$$f_i^a = \int_{\Gamma_t} N_i H f^t d\Gamma \tag{12}$$

In Equation (10), B is the matrix of shape function derivatives,

$$B_i^u = \begin{bmatrix} N_{i,x} & 0 \\ 0 & N_{i,y} \\ N_{i,x} & N_{i,y} \end{bmatrix} \tag{13}$$

$$B_i^a = \begin{bmatrix} (N_i H)_{,x} & 0 \\ 0 & (N_i H)_{,y} \\ (N_i H)_{,x} & (N_i H)_{,y} \end{bmatrix} \tag{14}$$

3. Case Validation

3.1. Validation of the Method

In order to check the validity of the mesh, a comparison between the numerical results and the theoretical value will be presented in this section for stress intensity factors (SIFs) of the central cracked plate. A detailed geometry and boundary conditions for the specimen is displayed in Figure 3. The plate thickness is 10 mm, and tensile load $\sigma = 100$ Pa.

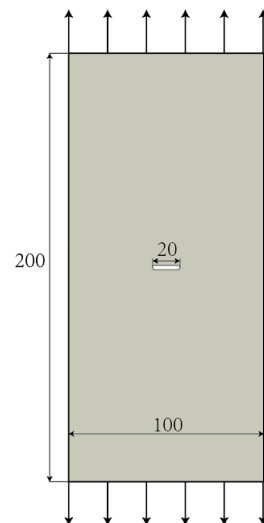


Figure 3. The central cracked plate (unit:mm).

The specimen SIFs at crack tips are defined as follows:

$$K_I = \sigma \sqrt{0.5\pi a} \left(1 + 0.5948\lambda^2 + 0.4812\lambda^4 \right) \tag{15}$$

where σ , a are the axial tensile load and the crack length in the specimen, respectively. And λ is given as $\lambda = a/W$, where W is the width of the central plate with crack.

The stress contour plot of σ_{yy} using different elements is shown in Figure 4. From the results, it can be deduced that the model with the mesh size of 2.8 mm is more accurate, however, the model with this mesh size will be more computationally costly.

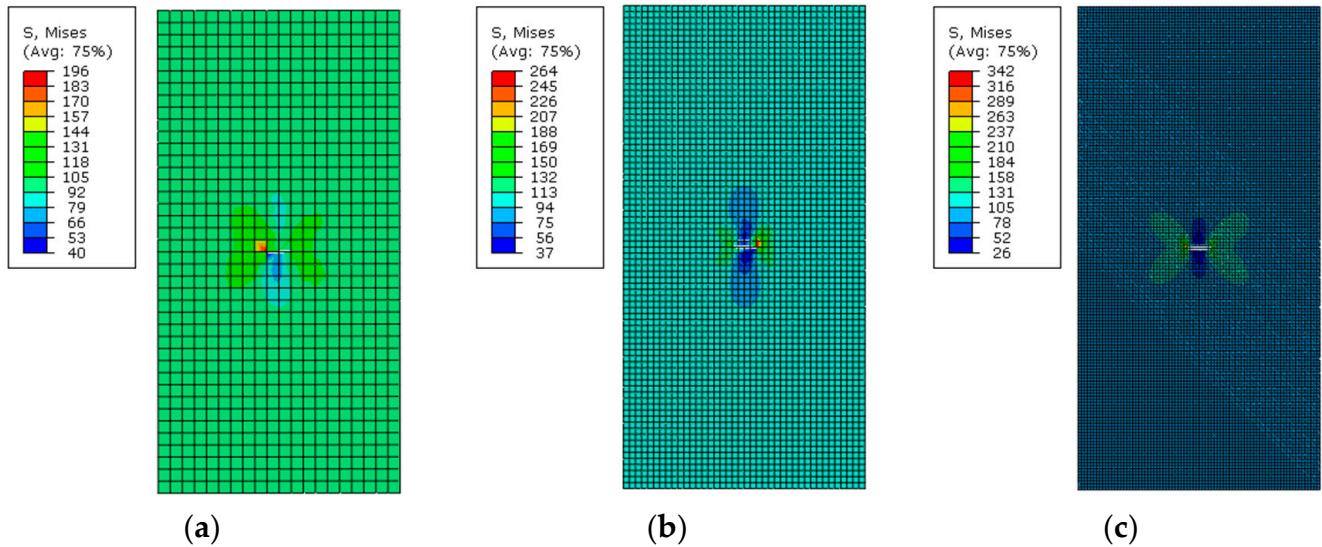


Figure 4. The stress contour plot of σ_{yy} for the central cracked plate in different element; (a) $h = 10$ mm; (b) $h = 5$ mm; (c) $h = 2.8$ mm.

Table 1 depicts the values of normalized SIFs at the tip of the center cracks for various elements. Material properties of stiffened plate model are shown in Table 2. For the central cracked plate, the theoretical value of SIFs is found as $574.1 \text{ MPa}\cdot\text{mm}^{1/2}$. As a reference numerical simulation, XFEM analysis by commercial software ABAQUS is conducted, and the SIFs value of crack tip is derived from the program provided by the software. When the average element of the model is taken as 5 mm, the numerical value of SIFs is found as $570.7 \text{ MPa}\cdot\text{mm}^{1/2}$. The normalized SIFs are 0.994, where the normalized SIFs are the ratio of the numerical value of SIFs to the theoretical value. The observation from Table 1 is that the SIF is 0.001 % more accurate than the theoretical value in the case where the mesh size is 5 mm, thus acceptable results can be obtained by using the 5 mm element size in the numerical simulation in this paper.

Table 1. Normalized SIFs in the central cracked plate.

Element Size	10	5	2.8
Normalized SIFs	1.205	0.994	1.005

Table 2. Material properties of stiffened plate model.

Young modulus	$E = 205.8 \text{ GPa}$
Poisson's ratio	$\nu = 0.3$
Max Principal Stress	$\sigma_{Max} = 235 \text{ MPa}$
Fracture Energy	$G_{Ic} = G_{IIc} = G_{IIIc} = 42.2 \text{ N/mm}$

3.2. Validation of the Present Method

In order to check the validity of the method, the numerical results and the experimental value will be compared in this section for fatigue crack growth rate of round compact tension specimen (RCT). The experiment of crack growth in RCT under cyclic loading is selected from the previous research work conducted by Wang et al. [30]. A detailed geometry and boundary conditions for RCT is displayed in Figure 5. Additionally, material properties of 2024-T4 aluminum alloy are shown in Table 3. The specimen's thickness is 3.7 mm, the initial crack length is $a_0 = 5$ mm, the maximum applied load $P_{max} = 3$ kN, and the stress ratio $R = 0.3$. The fixed crack growth increment is chosen as $\Delta a = 6$ mm.

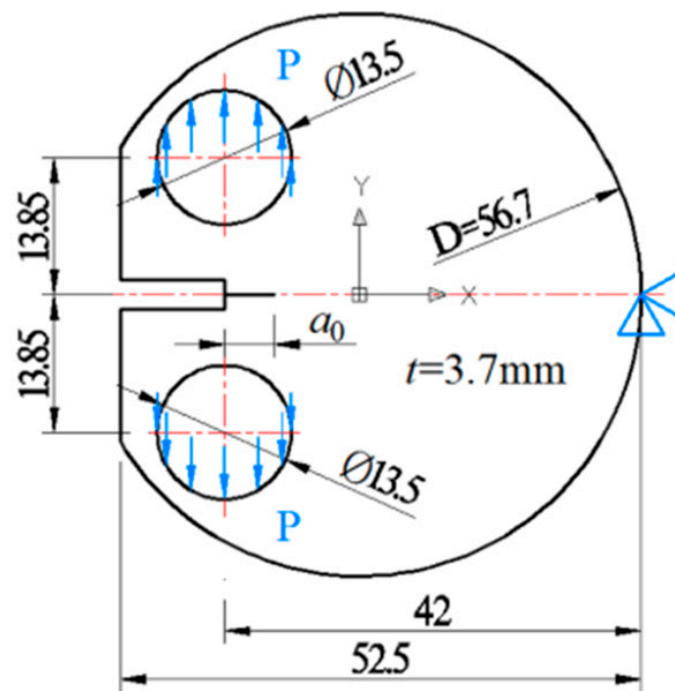


Figure 5. The round compact tension specimen (unit: mm).

Table 3. Material properties of 2024-T4 aluminum alloy.

Young modulus	$E = 73.1$ GPa
Poisson's ratio	$\nu = 0.33$
Tensile yield strength	$S_y = 324$ MPa
Paris exponent	$m = 3.738$
Paris constant	$C = 1.048 \times 10^{-8}$
Strain hardening constant	$\alpha = 0.314$
Strain hardening exponent	$n = 11.74$

The meshes used in XFEM is shown in Figure 6. It can be seen from Figure 6 that XFEM does not need to refine the mesh at the crack tip. Compared with the traditional finite element method, the extended finite element method uses a uniform mesh at the crack, which can save the calculation cost. The stress contour plots of σ_{yy} obtained by XFEM are shown in Figure 7. It can be noticed from Figure 7 that stress concentration occurs at the crack tip when the load is applied.

Figure 8 provides the comparison of numerical results and experimental data. From the results, it is observed that XFEM is in good agreement with the experimental data. Hence, this method can be used to simulate the crack growth behavior of stiffened plates.

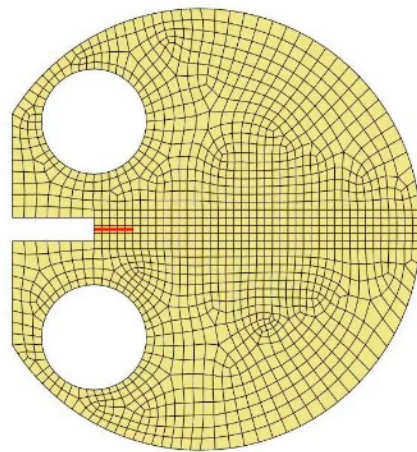


Figure 6. Meshing of the RCT specimen used in XFEM.

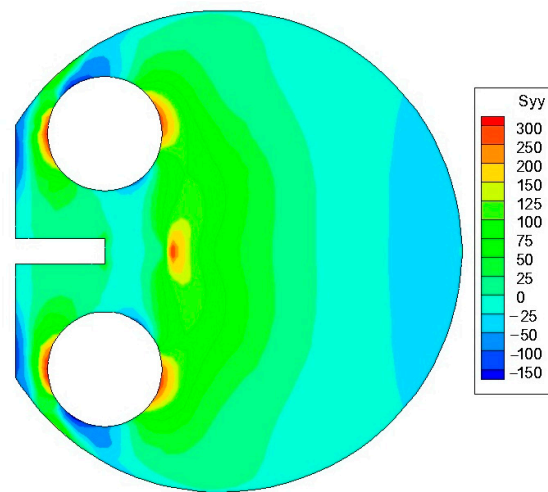


Figure 7. Stress contour plots of σ_{yy} for the RCT specimen. (Unit: MPa).

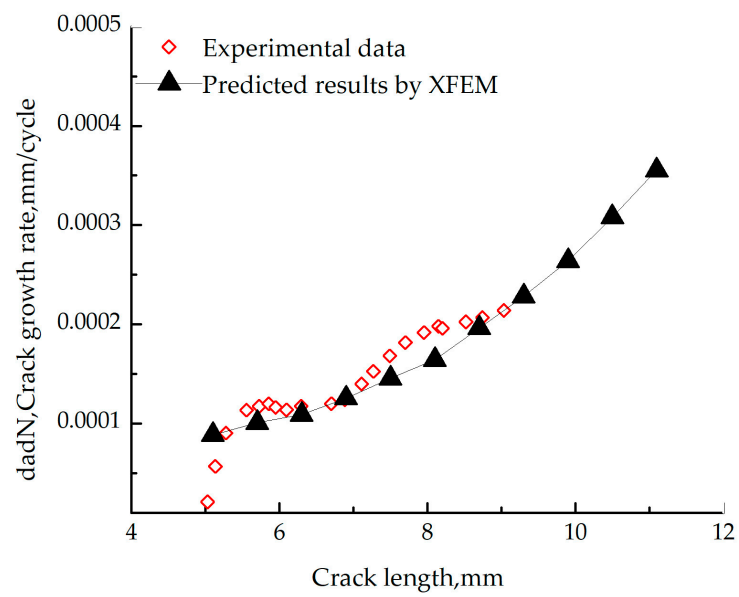


Figure 8. The comparison of numerical results and experimental data.

4. Numerical Case of Stiffened Plate

4.1. Description of the Models

Figure 9 shows the two stiffened plate models considered in the present study and material data are taken from the previous research work conducted by Peng and Yang [31], and material properties are shown in Table 2. The length, width and thickness of plate are denoted by a , b and t , respectively, and the web height and thickness of stiffener are represented by h_w and t_w . The cap-stiffened plate is used to simulate the bending model in order to fit the reality. The width and thickness of the cap are represented by a_c and t_c , respectively. The detailed geometric dimensions of stiffened plates are listed in Table 4.

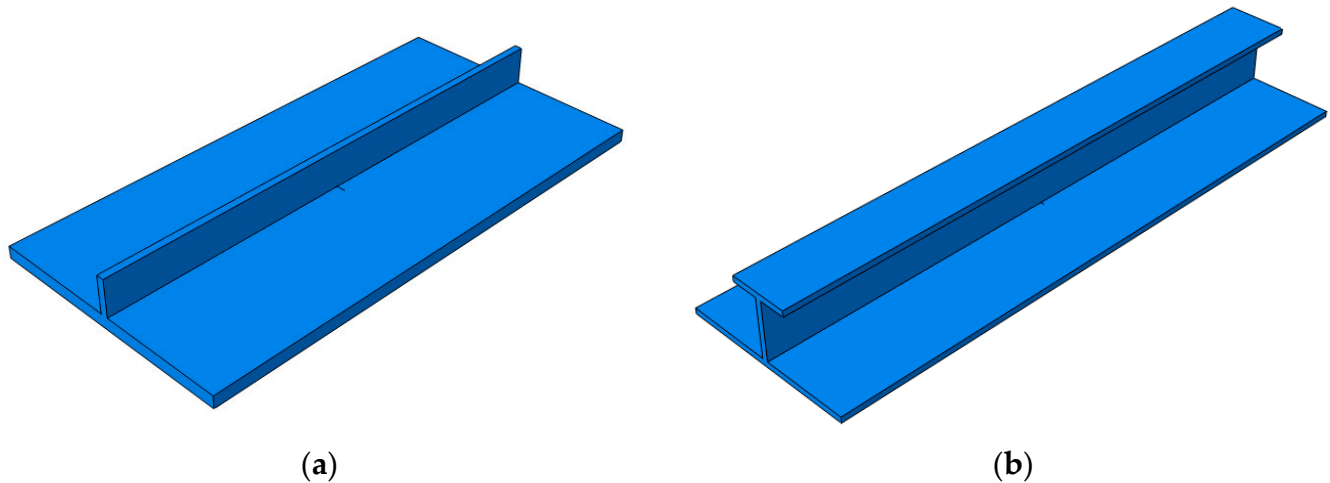


Figure 9. Geometries of stiffened panels: (a) tensile model; (b) bending model.

Table 4. Geometric dimensions of stiffened plates (unit: mm).

Models	a	b	t	h_w	t_w	a_c	t_c
tension	200	400	10	30	6		
bend	300	1000	10	75	6	100	6

4.2. Uniaxial Tension of Stiffened Plates with Central Cracks

The geometry and boundary conditions of the uniaxial tensile model in Figure 10 is taken for uniaxial tension of the stiffened plate’s analysis. The length of the uniaxial tensile model is 400 mm, and the central crack length is $a_0 = 20$ mm. Fully constrain the bottom of the stiffened plate and the x-direction of the plate to simulate the working condition of the tensile model. To facilitate the observation of the crack growth process, the average length of the element is 3 mm to located the crack tip inside the element. The model is subjected to tensile displacement load $S = 0.6$ mm, and the stress contour plot is depicted in Figure 11. As the figure shows, in the process of progressive displacement loading, stress concentration will occur at the crack tip whether on the plate or the stiffener. The displacement load required for crack initiation is 0.234 m, and later in the crack growth, the stress at the crack tip increases. The increasing speed of displacement load required by crack propagation gradually decreases, which means that when the crack propagates to the bottom plate of the tensile model, the crack resistance of the stiffened plate decreases.

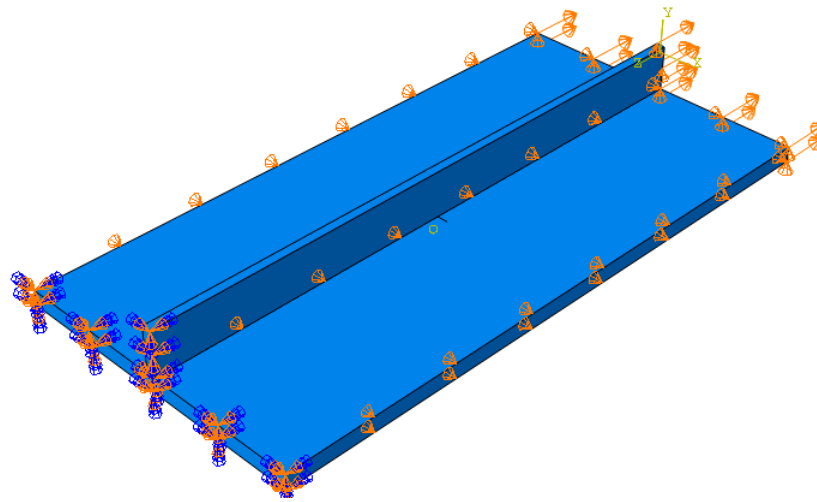


Figure 10. Geometry and boundary conditions of uniaxial tensile model.

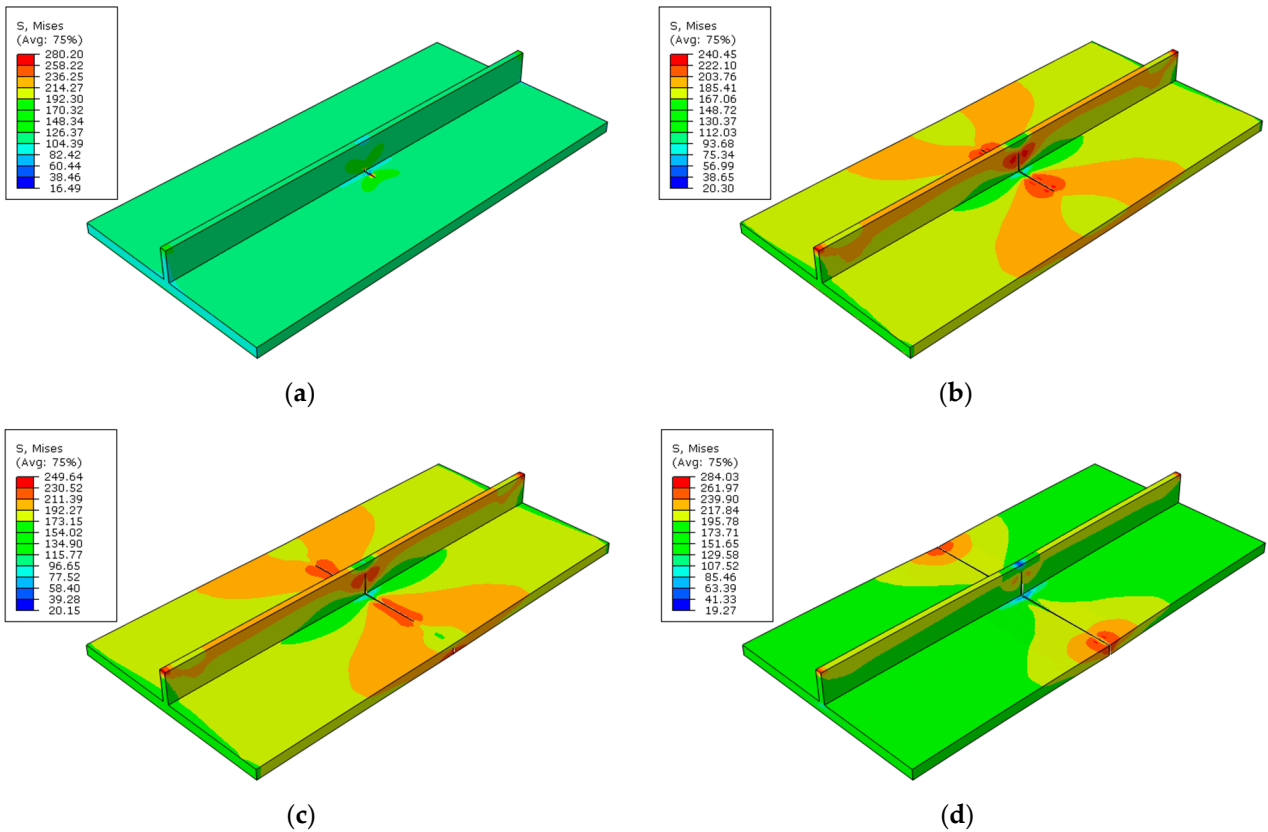


Figure 11. Stress contour plots for uniaxial tensile model; S is the displacement load under each state after conversion; (a) $S = 0.234$ mm; (b) $S = 0.370$ mm; (c) $S = 0.379$ mm; (d) $S = 0.391$ mm. (Unit: MPa).

The variation of the reaction force (RF) with time is depicted in Figure 12. It is concluded that when the crack of the bottom plate expands, the reaction force is linear with displacement load. When the bottom plate is completely damaged, the reaction force drops sharply, and the maximum reaction force is found as 441.31 kN. Until the stiffened plate breaks, and the reaction force reduces to 0.

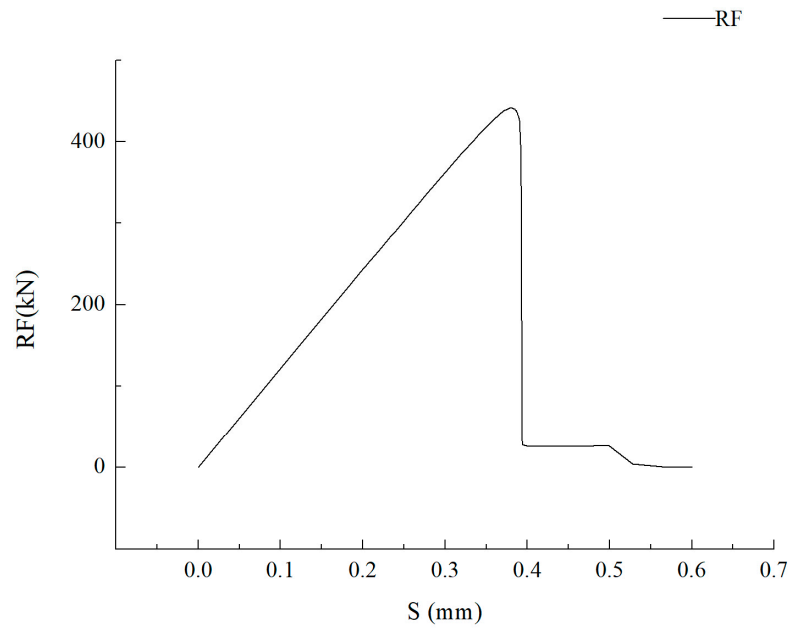


Figure 12. The relation of the reaction force of tensile model with displacement load.

4.3. Four-Point Bending of Stiffened Plate with Central Crack

A geometry and boundary conditions of four-point bending model in Figure 13 is taken for bending of stiffened plate’s analysis. The four-point bending model is simulated by constraining the support in the x and y directions, and applying the displacement load 200 mm away from the crack. In order to load the bending displacement, the stiffened plate is attached with a cap, the thickness, width and length of which are 6 mm, 100 mm, and 1000 mm, respectively. The model is subjected to tensile displacement load $S = 5$ mm, and the stress contour plot is depicted in Figure 14. It can be observed from Figure 14 that with the growth of the central crack of the stiffened plate, the stress at the crack tip also increases. The displacement load required for crack initiation is 0.88 m. Later in the growth of the crack, the increased rate of displacement load becomes lower. Therefore, with only a small amount of displacement load added, the crack will growth rapidly until the bottom plate of four-point bending model is broken.

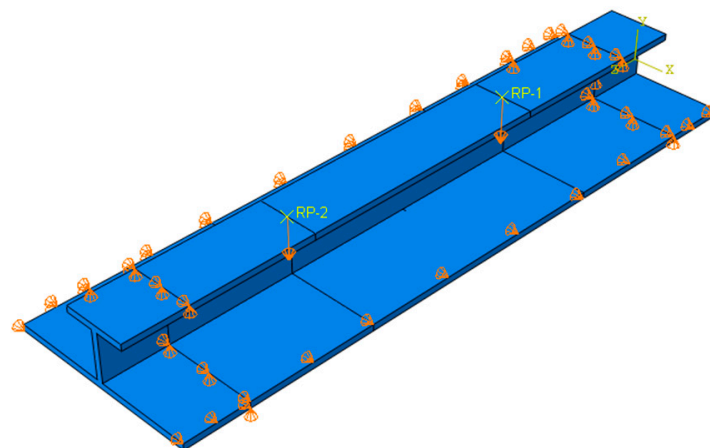
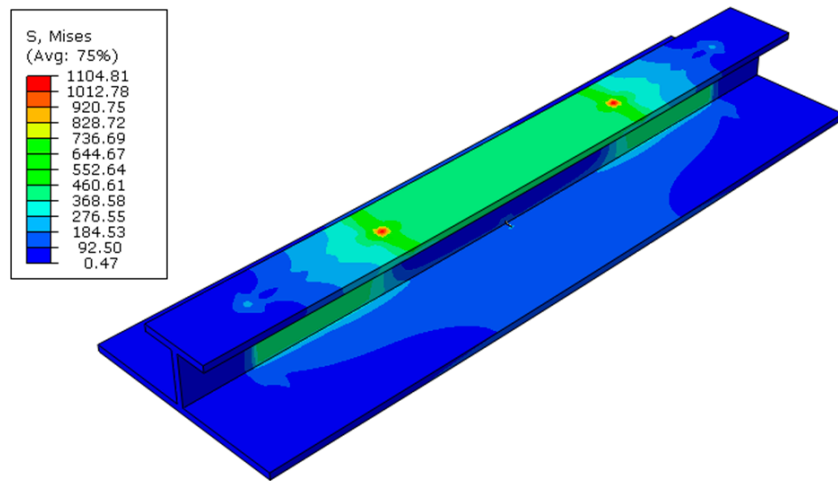
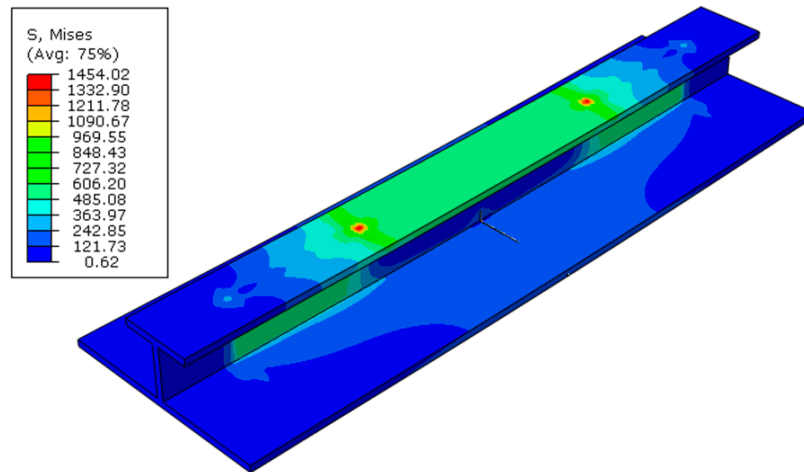


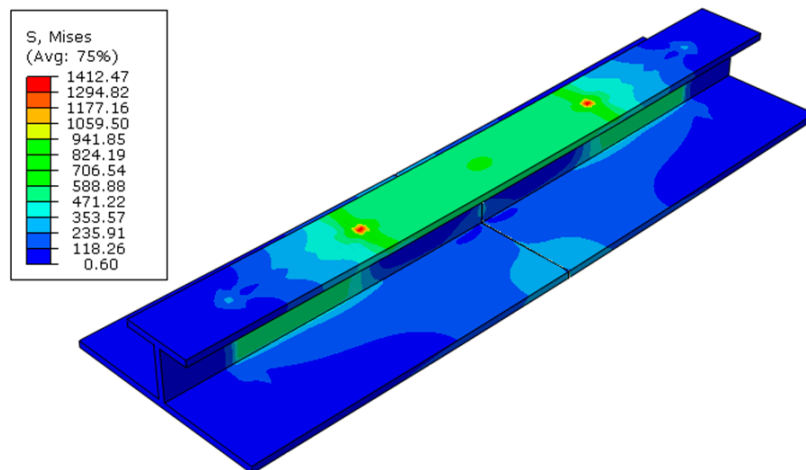
Figure 13. Geometry and boundary conditions of bending model.



(a)



(b)



(c)

Figure 14. Stress contour plots for bending model; S is the displacement load under each state after conversion; (a) $S = 0.88$ mm; (b) $S = 3.310$ mm; (c) $S = 3.365$ mm. (Unit: MPa).

The relationship between the reaction force of the bending model and the loading displacement is shown in Figure 15. The curve shapes of the reaction force versus the loading displacement are similar to the uniaxial tensile model. During crack growth, the reaction force and displacement load show a linear relationship, and the maximum reaction force is found as 264.4 kN. When the bottom plate is destroyed, the reaction force decreases rapidly, which means that the crack resistance of the stiffened plate decreases, until the stiffened plate is destroyed, and the reaction force reduces to 0.

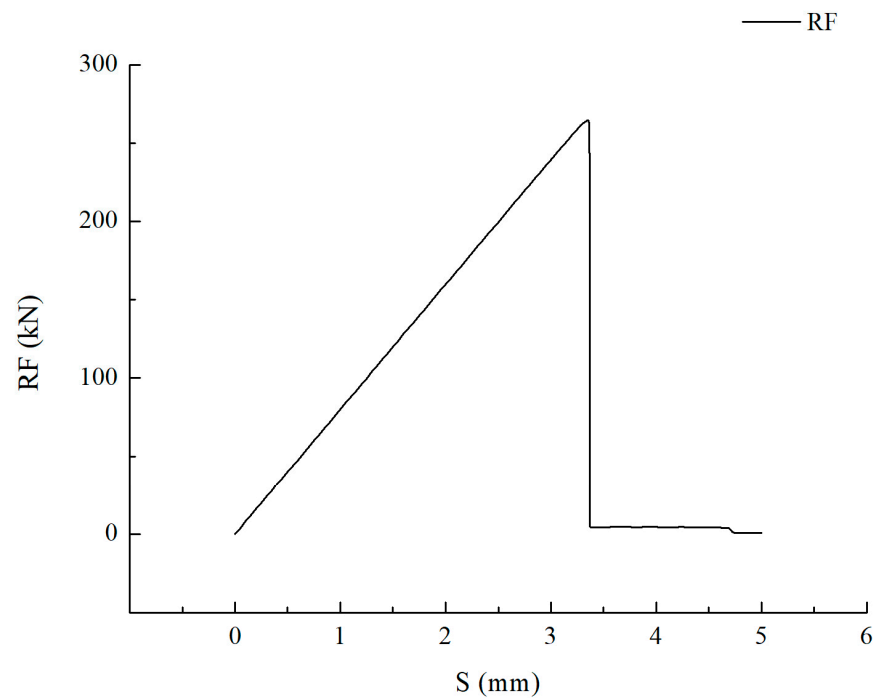


Figure 15. The relation of the reaction force of bending model with displacement load.

4.4. Influence of the Stiffener Size

The stiffener height has considerable influence on the ultimate strength of the stiffened plate. In this section, the plate geometry and material must be kept constant so as to examine the effect of different stiffener sizes on the residual ultimate strength of cracked stiffened plates. Three stiffener heights have been considered. Figure 16 shows the stress contour plots for crack propagation and the reaction force of the tension model under different stiffener sizes. It can be seen from Figure 15 that the stress is concentrated at the crack tip of stiffened plates with different heights of stiffeners during crack propagation, which also represents the correctness of this results. It is concluded that an increase in the stiffener height will significantly improve the ultimate bearing capability. This means that when the size of stiffeners increases, the crack resistance of tensile model will also be strengthened.

Figure 17 shows the stress contour plots for crack propagation and the reaction force of the four-point bending model under different stiffener sizes. It can be seen from Figure 17 that with the increase in the stiffener height in the four-bending model, the reaction force also increases. This shows that increasing the stiffener height in the bending model can increase the crack resistance of the stiffened plate.

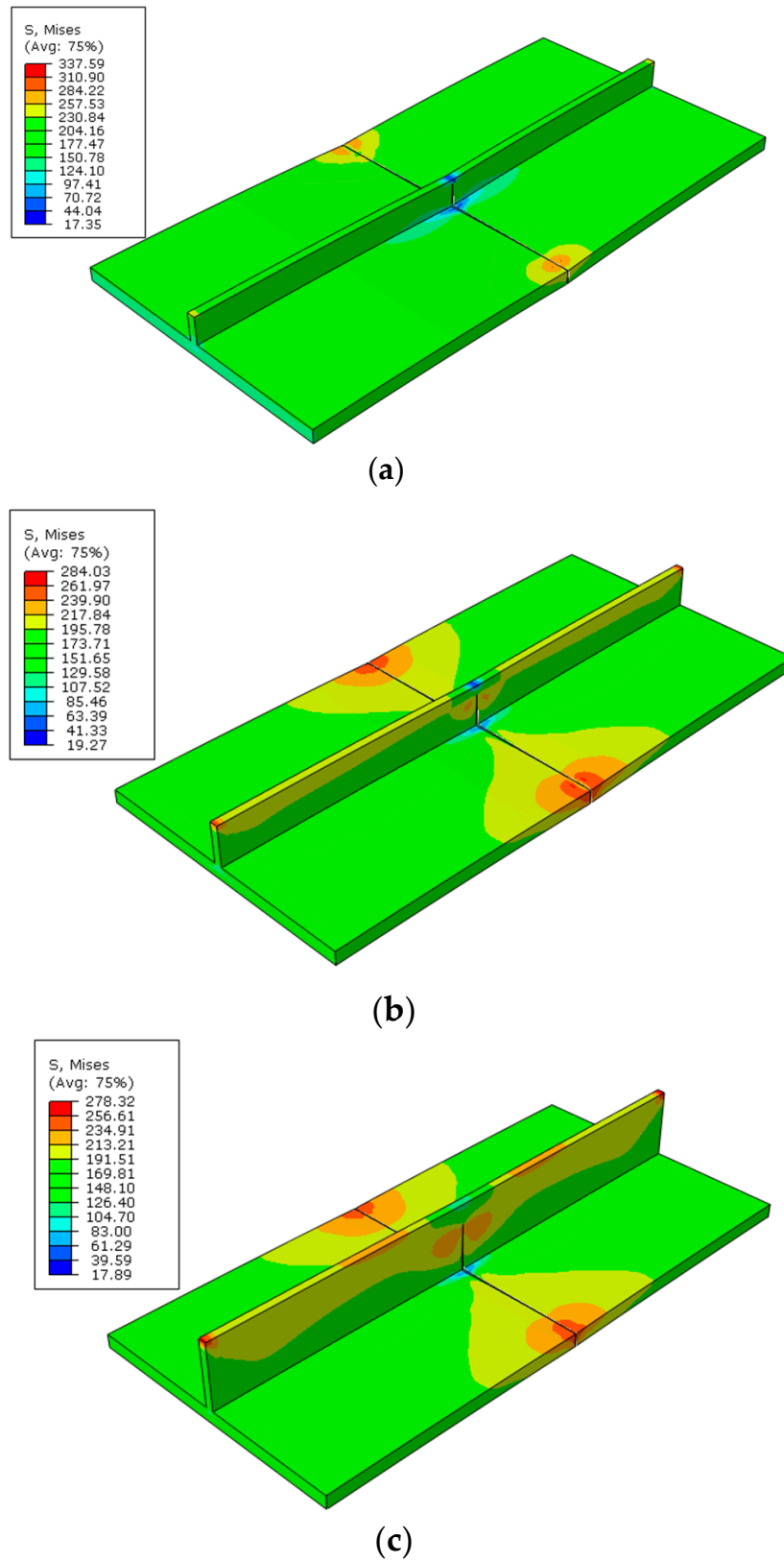


Figure 16. Stress contour plots for uniaxial tensile model in different stiffener sizes; (a) $h_w = 20$ mm, $RF = 399.5$ kN; (b) $h_w = 30$ mm, $RF = 421.7$ kN; (c) $h_w = 50$ mm, $RF = 450.7$ kN. (Unit: MPa)

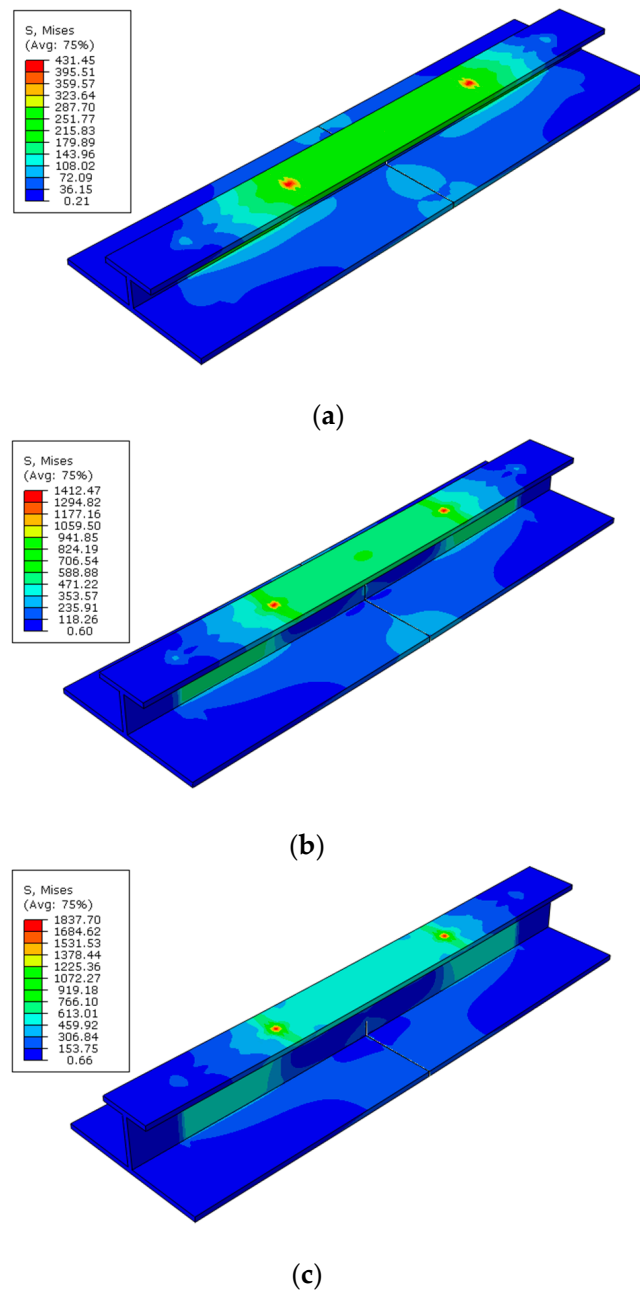


Figure 17. Stress contour plots for bending model in different stiffener sizes; (a) $h_w = 50$ mm, $RF = 74.4$ kN; (b) $h_w = 75$ mm, $RF = 255.4$ kN; (c) $h_w = 100$ mm, $RF = 335.3$ kN. (Unit: MPa)

5. Conclusions

In the present study, the residual ultimate strength of a stiffened plate with a central crack under displacement loading is simulated by XFEM. Two types of working condition, tension and bend were considered. In order to more reasonably evaluate the ultimate bearing capacity of stiffened plates with central cracks, the size of stiffeners is considered. Based on the results, the following conclusions and insights can be summarized.

- (1) For crack propagation, using XFEM, provided by software ABAQUS, to numerical analysis is in good agreement with theoretical value. XFEM can model crack growth with ease, as it precisely obtains results without refining the mesh.
- (2) The ultimate strength of central-cracked stiffened plates is reduced under displacement load both in tension and four-bending models. When the crack propagates, the stress is concentrated at the crack tip.

- (3) The stiffeners can restrain the cracking of specimens with initial cracks. Increasing the stiffener height, the ultimate residual strength of stiffened plates with central cracks improves accordingly for tension and bend models.

Author Contributions: Methodology, Z.C. and J.Z.; software, Z.C. and J.Z.; validation, G.L.; writing—original draft preparation, Z.C.; writing—review and editing, Z.C. and G.L. All authors have read and agreed to the published version of the manuscript.

Funding: This research was funded by [National Natural Science Foundation] grant number [No. 51909153] and the APC was funded by [National Natural Science Foundation (No. 51909153)].

Institutional Review Board Statement: Not applicable.

Informed Consent Statement: Not applicable.

Data Availability Statement: The data that support the findings of this study are available on request from the corresponding author, Guangzhong Liu, upon reasonable request.

Conflicts of Interest: The authors declare no conflict of interest.

References

- Nassiraei, H.; Mojtahedi, A.; Lotfollahi-Yaghin, M.A. Static strength of X-joints reinforced with collar plates subjected to brace tensile loading. *Ocean Eng.* **2018**, *161*, 227–241. [[CrossRef](#)]
- Nassiraei, H.; Rezadoost, P. Probabilistic analysis of the ultimate strength of tubular X-joints stiffened with outer ring at ambient and elevated temperatures. *Ocean Eng.* **2022**, *248*, 110744. [[CrossRef](#)]
- Xu, M.C.; Song, Z.J.; Zhang, B.W.; Pan, J. Empirical formula for predicting ultimate strength of stiffened panel of shipstructure under combined longitudinal compression and lateral loads. *Ocean Eng.* **2018**, *162*, 161–175.
- Feng, L.; Li, D.; Shi, H. A study on the ultimate strength of ship plate with coupled corrosion and crack damage. *Ocean Eng.* **2020**, *200*, 106950. [[CrossRef](#)]
- Li, D.; Chen, Z.; Li, J.; Yi, J. Ultimate strength assessment of ship hull plate with multiple cracks under axial compression using artificial neural networks. *Ocean Eng.* **2022**, *263*, 112438. [[CrossRef](#)]
- Luis, P.R.A.; Eduardo, T.L.J.; João, C.C.B. Probabilistic dipole BEM model for cohesive crack propagation analysis. *J. Braz. Soc. Mech. Sci. Eng.* **2022**, *44*, 485.
- Jobin, T.M.; Khaderi, S.N.; Ramji, M. Interaction of a rigid line inclusion with various discontinuities using experimental and numerical techniques. *Theor. Appl. Fract. Mech.* **2022**, *121*, 103482. [[CrossRef](#)]
- Gonçalves, D.C.; Sánchez-Arce, I.J.; Ramalho, L.D.C.; Campilho, R.D.S.G.; Belinha, J. Fracture propagation based on meshless method and energy release rate criterion extended to the Double Cantilever Beam adhesive joint test. *Theor. Appl. Fract. Mech.* **2022**, *122*, 103577. [[CrossRef](#)]
- Pu, N.; Zhang, Y.; Ma, W. A two-level nesting smoothed extended meshfree method for dynamic fracture analysis. *Eng. Fract. Mech.* **2022**, *275*, 108823.
- Tinh, Q.B.; Hung, T. Numerical simulations of dynamic fracture and fragmentation problems by a novel diffusive damage model. *Comput. Math. Appl.* **2022**, *125*, 193–212.
- Ramy, G.; Hidekazu, M.; Masakazu, S. Effects of specimen size and stress ratio on fatigue crack growth after a single tensile overload. *Ocean Eng.* **2022**, *261*, 112216.
- Zeng, Y.; Qu, Y.; Tan, Y.; Jiang, Y.; Gu, A. Analysis of fatigue cracking of orthotropic steel decks using XFEM. *Eng. Fail. Anal.* **2022**, *140*, 106536.
- Jena, J.; Singh, I.V.; Gaur, V. A numerical study of semipermeable cracks in Magneto Electro Elastic material using XFEM. *Eng. Fract. Mech.* **2022**, *275*, 108817. [[CrossRef](#)]
- Deng, H.; Yan, B.; Okabe, T. Fatigue crack propagation simulation method using XFEM with variable-node element. *Eng. Fract. Mech.* **2022**, *269*, 108533.
- Fries, T.P. A corrected XFEM approximation without problems in blending elements. *Int. J. Numer. Meth. Eng.* **2008**, *75*(5), 503–532. [[CrossRef](#)]
- Unger, J.F.; Eckardt, S.; Könke, C. Modelling of cohesive crack growth in concrete structures with the extended finite element method. *Comput. Method. Appl. Mech. Eng.* **2007**, *196*, 4087–4100. [[CrossRef](#)]
- Moës, N.; Belytschko, T. Extended finite element method for cohesive crack growth. *Eng. Fract. Mech.* **2002**, *69*(7), 813–833. [[CrossRef](#)]
- Khoei, A.R.; Nikbakht, M. Contact friction modeling with the extended finite element method (X-FEM). *J. Mater. Process. Tech.* **2006**, *177*, 58–62. [[CrossRef](#)]
- Khoei, A.R.; Nikbakht, M. An enriched finite element algorithm for numerical computation of contact friction problems. *Int. J. Mech. Sci.* **2007**, *49*(2), 183–199. [[CrossRef](#)]

20. Liu, Z.L.; Menouillard, T.; Belytschko, T. An XFEM/Spectral element method for dynamic crack propagation. *Int. J. Fract.* **2011**, *169*(2), 183–198. [[CrossRef](#)]
21. Daux, C.; Moes, N.; Dolbow, J.; Sukumar, N.; Belytschko, T. Arbitrary branched and intersecting cracks with the extended finite element method. *Int. J. Numer. Meth. Eng.* **2001**, *48*, 1741–1760. [[CrossRef](#)]
22. Sukumar, N.; Moes, N.; Moran, B.; Belytschko, T. Extended finite element method for three-dimensional crack modelling. *Int. J. Numer. Meth. Eng.* **2000**, *48*, 1549–1570. [[CrossRef](#)]
23. Yu, T.T.; Gong, Z.W. Numerical simulation of temperature field in heterogeneous material with the XFEM. *Arch. Civ. Mech. Eng.* **2013**, *13*, 199–208. [[CrossRef](#)]
24. Shi, X.H.; Zhang, J.; Guedes Soares, C. Numerical assessment of experiments on the residual ultimate strength of stiffened plates with a crack. *Ocean Eng.* **2019**, *171*, 443–457. [[CrossRef](#)]
25. Han, P.; Ri, K.; Yun, C.; Pak, C.; Paek, S. A study on the residual ultimate strength of continuous stiffened panels with a crack under the combined lateral pressure and in-panel compression. *Ocean Eng.* **2021**, *234*, 109265. [[CrossRef](#)]
26. Guo, Z.; Bai, R.; Lei, Z.; Jiang, H.; Liu, D.; Zou, J.; Yan, C. Experimental and numerical investigation on ultimate strength of laser-welded stiffened plates considering welding deformation and residual stresses. *Ocean Eng.* **2021**, *234*, 109239. [[CrossRef](#)]
27. Hu, K.; Yang, P.; Xia, T.; Song, Y.; Chen, B. Numerical investigation on the residual ultimate strength of cracked stiffened plates under extreme cyclic loads. *Ocean Eng.* **2022**, *244*, 110426. [[CrossRef](#)]
28. Cui, H.; Ding, Q. Ultimate strength and fracture failure of hull stiffened plates based on plastic accumulation under cyclic loading. *Ocean Eng.* **2022**, *261*, 112016. [[CrossRef](#)]
29. *ABAQUS Documentation*; Dassault Systemes: France, Paris, 2020.
30. Peng, Y.; Yang, P. Analysis of dynamic stress intensity factors for cracked stiffened plates based on extended FE method. *Int. J. Marit. Eng.* **2020**, *162*, 35–45. [[CrossRef](#)]
31. Wang, C.; Wang, X.; Ding, Z.; Xu, Y.; Gao, Z. Experimental investigation and numerical prediction of fatigue crack growth of 2024-T4 aluminum alloy. *Int. J. Fatigue* **2015**, *78*, 11–21. [[CrossRef](#)]

Disclaimer/Publisher’s Note: The statements, opinions and data contained in all publications are solely those of the individual author(s) and contributor(s) and not of MDPI and/or the editor(s). MDPI and/or the editor(s) disclaim responsibility for any injury to people or property resulting from any ideas, methods, instructions or products referred to in the content.